frontiers | Frontiers in Carbon

TYPE Original Research
PUBLISHED 27 May 2024
DOI 10.3389/frcrb.2024.1400664

OPEN ACCESS

EDITED BY
Lei Shi,
Sun Yat-sen University, China

REVIEWED BY
Guillaume Perry,
Sorbonne Universités, France
Shukun Chen,
South China University of Technology, China

*CORRESPONDENCE
Silviya P. Zustiak,
silviya.zustiak@slu.edu
Irma Kuljanishvili,
irma.kuljanishvili@slu.edu

RECEIVED 14 March 2024
ACCEPTED 10 May 2024
PUBLISHED 27 May 2024

CITATION
Luc E, Aziz B, Kim Y, Lespasio M, Jombo P, Zustiak SP and Kuljanishvili I (2024), Cell spreading and viability on single-walled carbon nanotube/zinc oxide nanowire heterostructures synthesized by chemical vapor deposition.
Front. Carbon 3:1400664.
doi: 10.3389/frcrb.2024.1400664

Cell spreading and viability on single-walled carbon nanotube/zinc oxide nanowire heterostructures synthesized by chemical vapor deposition

Emily Luc[1,2], Bashar Aziz[2], Yoosuk Kim[2], Marcus Lespasio[2], Philomena Jombo[1], Silviya P. Zustiak[1]* and Irma Kuljanishvili[1,2]*

[1]Department of Biomedical Engineering, Saint Louis University, St. Louis, MO, United States, [2]Department of Physics, Saint Louis University, St. Louis, MO, United States

Recent studies have shown the wide array of biomedical applications for nanomaterials such as single-walled carbon nanotubes (SWCNTs) and zinc oxide nanowires (ZnO NWs). SWCNTs are non-cytotoxic and have a varying range of mechanical, physical, and electrical properties useful to biomedical research. ZnO NWs are biocompatible, antibacterial, and exhibit piezoelectric properties that could stimulate cell growth. While recent research has been conducted using these nanomaterials independently, our study is focused on testing cell behaviors when seeded on SWCNTs, ZnO NWs and their heterostructure assemblies. ZnO NWs/SWCNTs heterostructures prepared via chemical vapor deposition (CVD) have not been used in biomedical applications to date. Here, we describe fabrication and characterization of the two nanomaterials independently and in a heterostructure formation. The NIH 3T3 fibroblast cells and U87 glioblastoma cells were seeded on all samples, including SiO_2/Si control/reference samples, and the cell growth was studied via fluorescence microscopy and scanning electron microscopy. The focus of this study was to evaluate cell spreading, filopodia extensions, and cell viability on these nanomaterial assemblies. Results indicated that cells were able to extend filopodia on all nanostructures, however cell spreading was more pronounced on SWCNTs, and cell viability was compromised on the ZnO NWs and the ZnO NWs/SWCNTs heterostructures. In addition, soluble compounds from the nanomaterials were tested to determine their cytotoxicity towards both NIH 3T3 and U87 cells. Results indicated a significant decrease in filopodia length, cell spreading, and cell viability when cells were exposed to ZnO NWs-conditioned cell media. These findings on cellular behavior involving SWCNTs, ZnO NWs, and ZnO NWs/SWCNTs heterostructure provide valuable information on the suitability of SWCNTs and ZnO NWs for future uses in biomedical applications.

KEYWORDS

cell viability, cell spreading, chemical vapor deposition synthesis, single-walled carbon nanotubes and zinc oxide nanowires, SWCNTs-ZnO NWs heterostructures

1 Introduction

Nanomaterials have been shown useful for a wide range of biomedical applications especially as a component to be integrated into micro- and nano-sized biological systems (Wang et al., 2009; Murali et al., 2021). Among the plethora of nanomaterials, one-dimensional carbon-based materials and zinc oxide (ZnO) nanostructures, such as single-walled carbon nanotubes (SWCNTs) and ZnO nanowires (ZnO NWs), have garnered attention for biomedical applications due to their unique physical properties and relative biocompatibility. SWCNTs exhibit unparalleled mechanical strength, boasting the highest Young's modulus and tensile strength among all nanomaterials as well as having directional conductivity stemming from a unique hexagonal crystal structure of rolled-up carbon sheets (Zhou et al., 2009). On the other hand, ZnO and ZnO NWs are semiconductive, photosensitive, and biodegradable, with high exciton binding energy and antibacterial properties due to their hexagonal wurtzite crystal structure (Ciofani et al., 2012; Zhang et al., 2012). Not surprisingly, both nanomaterials have been used in a variety of biomedical applications. While concerns with the toxicity of each nanomaterial have been raised, the use of a heterostructure surface coatings combining the two nanomaterials has not been explored in detail.

SWCNTs have been used in targeted cancer therapy, in glucose biosensors, and as substrates for neural growth, owing to their ability to promote cell adhesion and growth (Imaninezhad et al., 2018) or to penetrate cells and tissues and enable drug targeting and accumulation (Dineshkumar et al., 2015; Simon et al., 2019). However, the cytotoxicity of SWCNTs is of question, specifically for powdered nanomaterials that could be endocytosed by cells. A previous study has shown that SWCNTs toxicity to U87 glioblastoma cells is related to its downregulation of CDND2, a gene that promotes cell cycle progression, and upregulation of DUSP1 and DTNA, which are apoptosis regulator genes (Minchenko et al., 2016). Moreover, another study found that while glioblastoma growth was initially inhibited when exposed to CNTs, proliferation significantly increased over time (Imaninezhad et al., 2017; Parikh et al., 2020). On the other hand, studies of CNT-coated surfaces, unlike powered nanomaterials, have shown positive effects on non-cancerous cell behaviors including an increase of filopodia, cell spreading, proliferation and migration, and increased expressions of vinculin and talin (Bacakova et al., 2007), as well as increase in cell adhesion-related gene expressions (Ryoo et al., 2010). On the other hand, low doses of SWCNTs have been shown to affect astrocyte expression of proliferation and apoptosis related genes, thus evidencing SWCNTs possible genotoxic impact (Rudnytska et al., 2021).

ZnO NWs and ZnO nanostructures have been used in various biomedical applications, including sunscreen lotions, antibacterial coatings, biosensors, cancer-targeted drug delivery, and optical imaging (Hong et al., 2011; Sharma et al., 2022). ZnO can be cytotoxic to mammalian cells in a concentration-dependent manner due to direct cellular uptake and ion-shedding upon dissolution *in vivo*, where Zn^{2+} ions can affect cellular apoptosis mechanisms (Li et al., 2008; Wahab et al., 2011). It has been suggested that ZnO nanoparticles may be selectively localized in cancer cells from enhanced permeability and retention effect and electrostatic interactions, thus showing that they may selectively target cancer cells (Bisht and Rayamajhi, 2016). However, ZnO NWs appear to be biocompatible when used as coatings and/or presented extracellularly. For example, Cui et al. found that cells grown on ZnO NWs-covered polydimethylsiloxane (PDMS) microchips had better biocompatibility than those grown on hydrophobic PDMS alone (Cui et al., 2020).

One way to diversify functionalities and applications of individual nanomaterials and to achieve improved biocompatibility and enhanced properties is to form heterostructures of such nanomaterials. Various heterostructures have been extensively studied in nanoscience but less work has been done on determining their effect on cells for biomedical applications. One notable example of incorporating heterostructures *in vivo* has been titanium and strontium nanoparticle-nanotube heterostructures. These were made to use titanium's osseointegration property with strontium's ability to decrease osteoresorption and it was suggested that such heterostructures may be used in bone implants in clinical settings (Yin et al., 2017). CNTs and ZnO NWs heterostructures have been used previously in high performance electrodes for superconductor applications (Al-Asadi et al., 2017), as chemical sensors (Shooshtari et al., 2022), and as photocatalysts (Dai et al., 2012), but their effect on cells has not been explored in detail.

When combining ZnO and CNTs, the ZnO/CNTs hybrid materials can provide a new platform for utilizing a spectrum of properties, which can be used simultaneously in multimodal environments in the biomedical field. Still, the development of ZnO/CNTs nanocomposites for biomedical applications is in its infancy, possibly due to toxicity concerns for both ZnO and CNT-nanopowders. In contrast, one-dimensional nanowire heterostructures, such as ZnO NWs/SWCNTs when grown directly on the substrates can offer a new testing environment for the evaluation of cell behaviors. To the best of our knowledge, ZnO NWs/SWCNTs heterostructures in pristine highly crystalline formations grown directly on top of each other have not been used in biological applications, thus further emphasizing the need and the purpose of this study. The preparation of ZnO NWs/SWCNTs heterostructures directly grown on a substrate, a departure from conventional studies utilizing dispersed or powdered forms, was made possible using a novel chemical vapor deposition (CVD) method recently developed by our team (Schaper et al., 2021). This study aims to investigate the impact of the heterostructures on cells by analyzing the morphology, frequency of filopodia, and viability of NIH 3T3 mouse fibroblast and U87 glioblastoma cell lines. We hypothesized that the heterostructure of ZnO NWs/SWCNTs could work in synergy where SWCNTs could promote non-cancerous cell growth, and ZnO NWs could suppress cancerous cell growth, thus utilizing uniqueness of both nanomaterials to interact with cells in a specific and/or selective way. Our studies indicated that cells were able to adhere to the heterostructures as well as to both SWCNTs and ZnO NWs individually but, at the same time, also indicated to the possible toxicity of Zn^{2+} ions released from the ZnO NWs towards both normal and cancer cell types. Our work did not show selective ZnO NWs toxicity towards cancer cells, when used

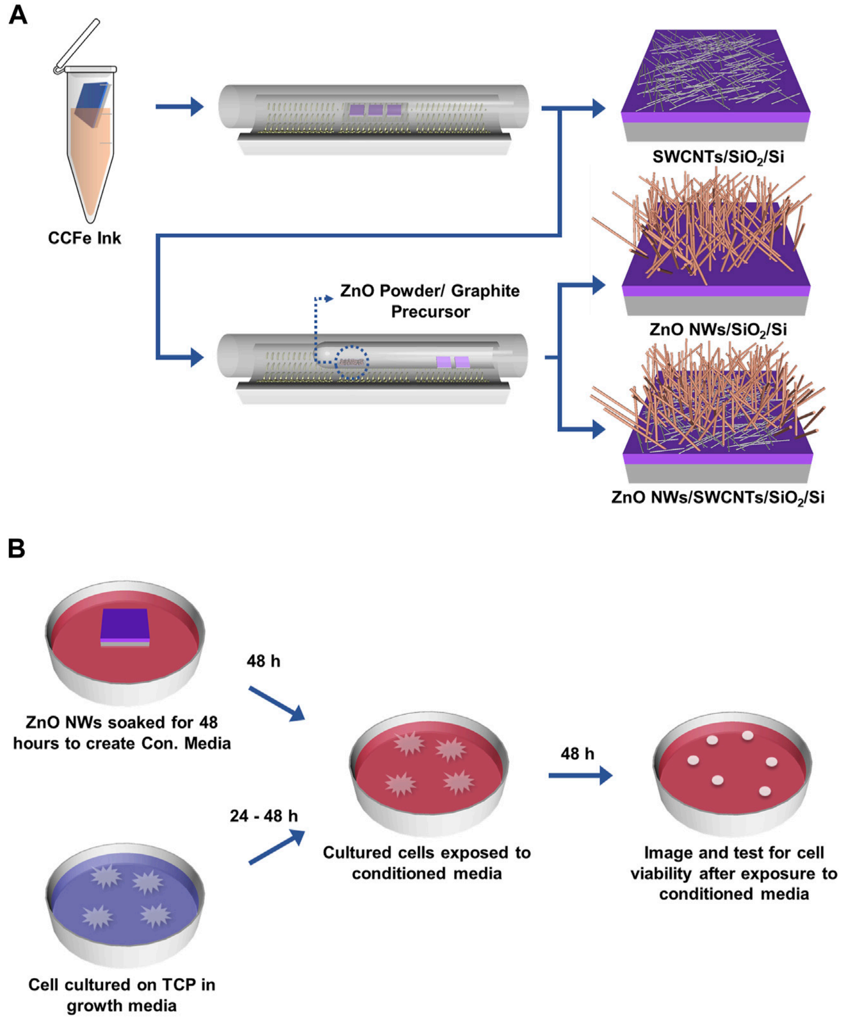

FIGURE 1
Schematic of CNTs and ZnO NWs and heterostructure synthesis on SiO_2/Si and ZnO NWs conditioned media preparation. **(A)** CVD synthesis of SWCNTs, ZnO NWs, and ZnO NWs/SWCNTs. **(B)** ZnO NWs are soaked for 48 h in complete cell medium to prepare ZnO NWs conditioned media (Con. Media). Cells cultured on TCP for 24 h were exposed to Con. Media for 48 h.

alone or in the heterostructure, underscoring the need for further research.

2 Materials and methods

2.1 Chemical vapor deposition synthesis of SWCNTs

SWCNTs were synthesized following a protocol previously established by our team (Figure 1A) (Kuljanishvili et al., 2009; Schaper et al., 2021). Briefly, SiO_2/Si chips of 5 x 5 mm were cut from SiO_2/Si wafers (UniversityWafer, South Boston, MA, P/B, (100), resistivity: 1–5 mΩ.cm, 300 nm of Thermal Oxide) and cleaned in order of acetone, isopropanol, and deionized (DI) water via sonication (BRANSON, Model #2800, 40 kHz) for 3 min in each solvent. Chips were then placed in an ultraviolet (UV) ozone system (Novascan PSD Pro Series Digital UV Ozone System, Boone, IA, United States) for 3 min to render optimal hydrophilicity. Each chip was dipped into custom composite Fe-based (CCFe) precursor ink for 10 s to ensure the entire surface was properly coated. The precursor ink consisted of 6 parts master solution (Iron (III) nitrate nonahydrate ($Fe(NO_3)_3·9H_2O$) (Sigma-Aldrich, St. Louis, MO, United States, 99.99% purity): 3 parts DI water: 2 parts N,N-dimethylformamide (Sigma-Aldrich, St. Louis, MO, United States, ≥99% purity): 1 part Glycerol (Sigma-Aldrich, St. Louis, MO, United States, ≥99.0% purity). The chips were gently dried with the nitrogen gas and placed onto a quartz holder/boat, which was subsequently inserted into a quartz tube (Technical Glass Products, Painesville, OH, United States) inside a CVD three-zone furnace (Thermo Fisher Scientific Lindberg/Blue M, Waltham, MA, United States). The home-built CVD system is equipped with a mass flow controller (Sierra Instrument, Monterey, CA. United States) to manage the precise gas flow. The CVD growth process involved preconditioning of the catalysts at 365°C under argon (Ar) and hydrogen (H_2) gas mixture at a 1:0.5 gas ratio for 67 min followed by the growth at 900°C with methane (CH_4) precursor gas for 18 min and allowed to cool down under protection of Ar/H_2 gas mix with 1:

0.5 gas ratio. During the growth stage the mixture of $CH_4/H_2/Ar$ gas with the flow rates of 900/60/140 (sccm), respectively, was used in the CVD chamber.

2.2 CVD synthesis of ZnO NWs and ZnO NWs/SWCNTs

ZnO NWs and ZnO NWs/SWCNTs heterostructures were synthesized following a protocol previously established in our lab (Figure 1A) (Alameri et al., 2017a; Schaper et al., 2021). Briefly, to make ZnO NWs and ZnO NWs/SWCNTs, graphite (Alfa Aesar, Haverhill, MA, United States, 99.999%) and ZnO powder (Alfa Aesar, Haverhill, MA, United States, 99.999% purity) were used as precursors. 35 mg of each reagent mixed and placed into a small quartz boat (Technical Glass Products, Painesville, OH, United States). This boat was further placed into a quartz tube with one closed end, along with SiO_2/Si samples placed near the opening on the closed-end tube. ZnO NWs were grown at 930°C under Ar gas protection inside the CVD chamber. The synthesis of ZnO NWs/SWCNTs heterostructures involved growing the SWCNTs on the SiO_2/Si chips first, as described above, and subsequently growing the ZnO NWs directly on the SWCNTs, with no additional precursor catalyst thus creating seamless interface between the materials. All samples were used "as-grown" for all experiments without post-processing or surface treatments.

2.3 Nanomaterial characterization

Scanning electron microscopy (SEM; FEI Inspect F50, Lausanne, Switzerland) was used to visualize and evaluate nanomaterials. SWCNTs were imaged at 1.5 kV and ZnO NWs were imaged at 10 kV. Raman spectral measurements and analyses were also performed (Renishaw, InVia, Wotton-under-Edge, Gloucestershire, England) to determine the quality and crystallinity of the synthesized nanomaterials. Atomic force microscope (AFM; Park NX 10, Suwon, South Korea) in non-contact mode was used for carbon nanotube topographic imaging and to determine diameter of SWCNTs. Average length of SWCNTs and ZnO NWs were evaluated using ImageJ software (free download from the NIH at imagej.nih.gov). A home-built system assembled with trinocular stereo microscope equipped with a digital camera was used to take images of the sample surfaces for subsequent contact angle measurements. Briefly, 2 µL of DI water was dispensed on each sample, where samples were in ambient conditions during all measurements (with temperature and humidity maintained at 23°C and 20%, respectively). ImageJ software was used to measure the contact angle from the acquired images.

2.4 Cell maintenance

NIH 3T3 Cells (ATCC-CRL-1658™, ATCC, Manassas, VA) were maintained in Dulbecco's Modified Eagle's Medium (DMEM; Gibco ®, Bristol, RI). DMEM was supplemented with 10% heat-inactivated fetal bovine serum (FBS, Sigma-Aldrich ®, St Louis, MO), 100 units/mL Penicillin and 100 µg/mL Streptomycin (1% pen/strep). Cells were utilized between passages 7 to 18 and kept in a 37 °C and 5% CO_2 incubator. U87 MG glioblastoma cells (ATCC-HTB-14™) were maintained in Roswell Park Memorial Institute (RPMI) 1,640 medium supplemented with 10% FBS and 1% pen/strep. For both cell types, medium was refreshed every 2–3 days and cells were passaged when 80% confluence was reached by exposure to 0.05% trypsin/0.02% ethylenediamine triacetic acid (EDTA).

2.5 Cell seeding on nanomaterials

To prevent non-specific cell attachment, 1% bovine serum albumin (BSA, Thermo Fisher Scientific, Waltham, MA) in phosphate buffered saline (PBS) buffer was pipetted onto the wells of 48-well plates (100 µL/well) and incubated for 30 min, then carefully rinsed with PBS. SiO_2/Si chips with or without grown nanomaterials were sterilized by a dip in 200 proof ethanol for 1 min, dried completely in a tissue culture hood. And then placed inside the wells of the pre-treated 48-well plates (one chip per well). U87 and NIH 3T3 cells were then seeded on top of the chips at ~5,000 cells per well with 200 µL of cell medium supplemented with 10% FBS and 1% pen/strep. Cells were cultured for 24 h on top of each chip in a humidified incubator at 37°C and 5% CO_2.

2.6 Cell imaging via SEM and analysis of cell filopodia

For SEM imaging, U87 and NIH 3T3 cells on chips with and without nanomaterials were first fixed with 2.5% glutaraldehyde in 0.1 M sodium cacodylate buffer with 2% sucrose and 2 mM $CaCl_2$ (pH 7.25) and then with 1% osmium tetroxide (Electron Microscopy Sciences, Hatfield, PA) in 0.1 M sodium cacodylate buffer with 2% sucrose to preserve membrane structures. After fixation, the cells were consecutively dehydrated in 30%, 50%, 75%, 95%, and 100% ethanol. SEM (FEI Inspect F50, Lausanne, Switzerland) images were taken at 1.5 kV high voltage, and ×750 magnification. SEM images were used to observe cell filopodia with respect to nanomaterials to give qualitative data on cell interactions with the nanomaterials.

2.7 Cell imaging via microscopy and analysis of cell viability and morphology

For microscopy imaging, U87 and NIH 3T3 cells on chips with and without nanomaterials were either imaged live or fixed with 2.5% glutaraldehyde in 0.1 M sodium cacodylate buffer with 2% sucrose and 2 mM $CaCl_2$ (pH 7.25). For fluorescence imaging, live cells were stained with Cell Tracker (CellTracker™ Green CMFDA dye, Thermo Fisher, Scientific) following the manufacturer's procedure. Microscopy images were taken with a reflected light microscope (Nikon, Optiphot 66, Minato City, Tokyo, Japan) at ×20 magnification. Microscopy images were analyzed in ImageJ and used to measure cell area and calculate cell shape factor (Eq. 1), where a shape factor value of 1 represents cells of a circular shape, while values approaching 0 indicate elongated cells.

$$Shape\ Factor = \frac{4\pi(Area)}{Perimeter^2} \tag{1}$$

Cell viability was measured with a LIVE/DEAD™ Viability/Cytotoxicity Kit, for mammalian cells (Thermo Fisher Scientific), where live cells were stained green with Calcein AM and dead cells were stained red with ethidium homodimer-1 (EthD-1). The stains were applied at concentrations of 4 μM for EthD-1 and 2 μM Calcein AM added directly to the cell media, and cells were incubated at 37°C for 30 min before imaging. In certain cases, CellTracker was used instead of Calcein AM to allow for better visualization of the whole cell while still staining all cells green. For live/dead staining, care was taken to rinse the cells gently as to cause minimal detachment of dead cells prior to staining. However, it is possible that some dead cells were detached from the substrate and thus, not included in the total cell viability calculation, skewing the results slightly towards higher than actual cell viability. Percent viability was calculated by counting the total cells stained green with CellTracker or the live cells stained green with Calcein AM and the dead cells stained red with EthD-1 as:

$$\%\,Cell\ Viability = \frac{Total\ Cells - Dead\ Cells}{Total\ Cells} * 100 \tag{2}$$

2.8 ZnO NW conditioned media preparation and analysis of cell response

ZnO NWs conditioned media (Con. Media) was prepared by soaking ZnO NW grown on SiO_2/Si chips in 200 μL of either DMEM or RPMI 1640 media for 48 h. U87 and NIH 3T3 cells cultured on tissue culture polystyrene (TCP) in complete medium (10% FBS, 1% pen/strep) for 24 h were then exposed to ZnO NWs conditioned media for 48 h and imaged under optical microscope at 0, 24, and 48 h to observe cell spreading (Figure 1B). Additionally, to determine whether the presence of SWCNTs affected cell viability in ZnO NWs conditioned media, and to exclude the possibility that the SWCNTs presence was affecting cell spreading/viability, cells were cultured on SiO_2/Si chips for the reference (as control) and SWCNTs grown on SiO_2/Si chips and positioned in the wells of multi-well plates. At 24 and 48 h, both the cells that were on the well bottom (in the same well plates as SiO_2/Si chips and SWCNTs; labeled as TCP) and the cells on top of the SiO_2/Si chips and SWCNTs were imaged. Images of cells on TCP (on the well bottom) were taken through an inverted microscope (Zeiss, Axiovert 200M, Oberkochen, Baden-Württemberg, Germany). Cells on the SiO_2/Si chips and SWCNTs were stained with 4 μM of EthD-1 and 2 μM Calcein AM for 30 min at 37 °C and imaged with an upright fluorescent microscope as described above. Cell viability was calculated via Eq. 2.

Dynamic light scattering (DLS; Malvern Panalytical, Zetasizer Nano ZS, Malvern, United Kingdom) analysis was performed for the conditioned media to determine whether ZnO NW particulates were released in the medium during soaking. Particulate size was compared between conditioned and unconditioned media.

2.9 Zn^{2+} concentration determination in conditioned media

Conditioned media analyses were performed on ZnO NWs and ZnO NWs/SWCNTs samples grown by CVD on SiO_2/Si before and after they were soaked in media. A total of 6 samples were tested, 4 of which were ZnO NWs and 2 samples were ZnO NWs/SWCNTs heterostructures. The Zn^{2+} concentration in the cell media released from the ZnO NWs was approximated as follows: the average number of ZnO NWs were calculated per unit area of the samples/chips such as ZnO NWs/SiO_2/Si and ZnO NWs/SWCNTs/SiO_2/Si, using SEM imaging. Average length and diameter of the NWs were also determined from SEM images, thus providing us with the unit of measure of an average estimated volume of the ZnO materials to further determine the concentration of Zn^{2+} ions in each medium. For consistency, SEM images of all samples were processed in the same way: dividing each chip into three-by-three quadrants, thus analyzing nine regions. In accordance with the experimental details above, the nanomaterials were soaked in complete cell media for 48 h before being dried and reimaged in the same quadrants as before. SEM image files were imported into MATLAB and ImageJ software was used to evaluate percent coverage. The amount of material before and after dissolution was compared and from there, the percent dissolution of ZnO was estimated.

2.10 Statistical analysis

Data points are shown as average ± standard deviations from 3 independent experiments with up to 3 samples per experiment. For cell analysis from microscopy images, multiple images were taken per sample and up to 150 cells were analyzed per condition. When testing for statistical difference between experimental conditions, GraphPad Prism software was utilized to conduct two-wailed t-tests between 2 conditions, and a one-way ANOVA with *post hoc* Tukey test to compare greater than 2 conditions. Significance is reported as $p < 0.05$.

3 Results

3.1 Nanomaterial characterization

Nanomaterials undergo significant morphological changes upon incorporation into heterostructures, necessitating precise characterization to quantify their quality and morphology alterations. This study employed SEM imaging to verify the morphology of individual nanomaterial components. SWCNTs grew horizontally as monolayers, exhibiting lengths ranging from 2.6 to 17.6 μm (Figure 2A). On the other hand, ZnO NWs grew preferentially in vertical orientations in densely packed arrangements resembling forests. The length and diameter of ZnO NWs ranged from 0.9 to 3.2 μm and 47.3–99.2 nm, respectively (Figure 2B; Supplementary Figure S1A, B). The percentage coverage of SWCNTs on SiO_2/Si was observed to trend lower than that of ZnO NWs and the heterostructures. This phenomenon could be attributed to the fact that some

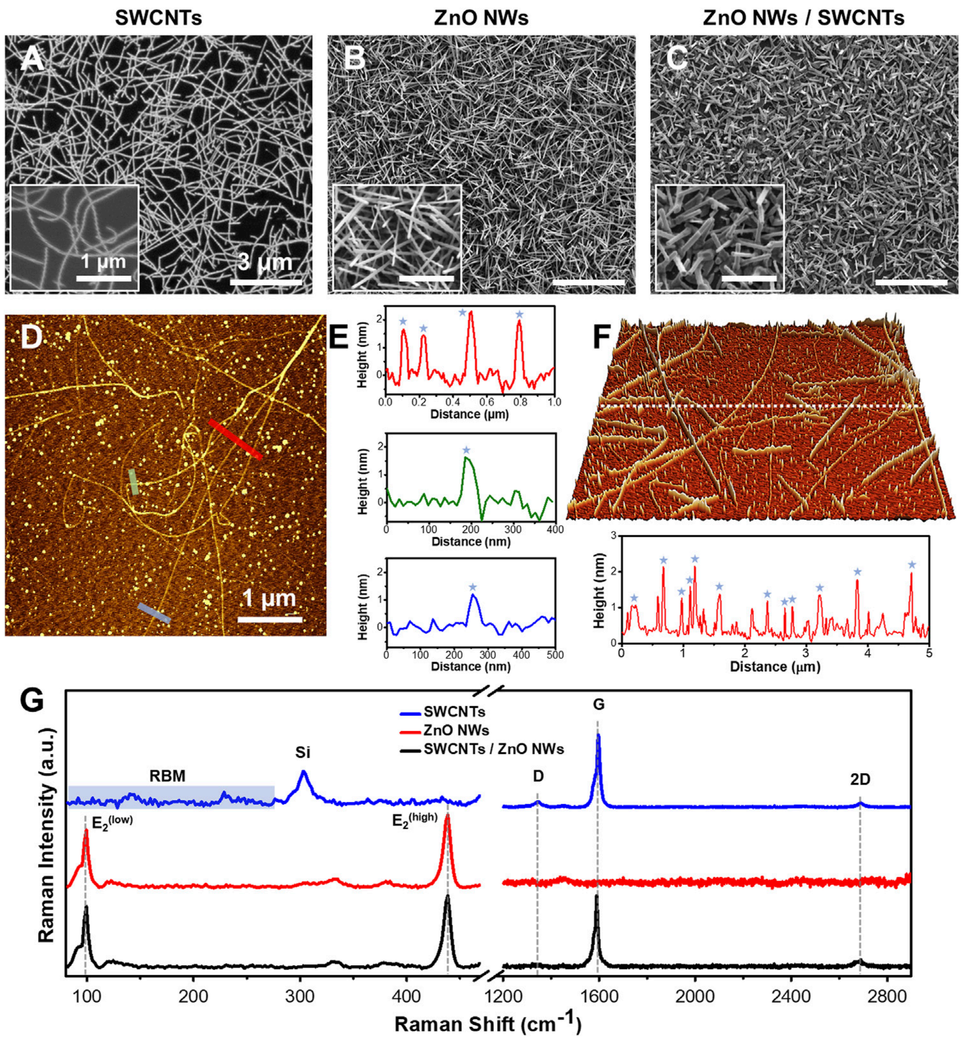

FIGURE 2
SEM, AFM, and Raman of SWCNTs, ZnO NWs, and SWCNTs/ZnO NWs heterostructures. SEM images of **(A)** SWCNTs, **(B)** ZnO NWs, and **(C)** SWCNTs/ZnO NWs heterostructures on SiO_2/Si substrate demonstrating uniformity and high density. Scale = 3 μm. Insets are high-magnification SEM images of each sample. Scale = 1 μm. **(D)** AFM image of SWCNTs with **(E)** line profiles showing the height of the SWCNTs (blue star) at the specified color-coded locations. **(F)** 3D AFM topographic image (for a 5x5 μm square area) of SWCNTs grown on SiO_2/Si substrate with a line profile shown below. **(G)** Raman spectral plots of representative spots on each sample of each nanomaterial featuring G and D and 2D bands for SWCNTs presence and the E_2^{low} and E_2^{high} peaks for ZnO NWs presence. RBM modes in the SWCNTs Raman plot can also be seen at the low-frequency range.

catalytic particles (as seen Figures 2D, F) did not participate in SWCNTs growth but would have been reactivated during ZnO NWs to nucleate ZnO NWs. Furthermore, in the fabricated heterostructures, consisting of ZnO NWs grown on SWCNTs, only the ZnO NWs were discernible (Figure 2C), underscoring the successful integration of the two nanomaterial components into a heterostructure configuration. The length and diameter of ZnO NWs grown on SWCNTs ranged from 0.5 to 1.5 and 66.5–133.5 nm, respectively (Supplementary Figures S1C, D).

The contact angles measurements conducted on the surfaces of the nanomaterials were conducted to evaluate their surface wettability (Supplementary Figure S2). The reported values represent averaged values from six samples. The average contact angles of SWCNTs, ZnO NWs, and ZnO NWs/SWCNTs were determined to be 79.5°, 119.6°, and 128.5°, respectively. Notably, ZnO NWs and ZnO NWs/SWCNTs values can be categorized as hydrophobic, attributed to their high aspect ratio, vertical orientation, and subsequently inherent high surface roughness (Mohammad Karim, 2023). Further, wettability of ZnO NWs is contingent upon the crystallographic orientation of the NWs where the surface of ZnO can be categorized as polar and non-polar (Mardosaitė et al., 2021). The nonpolar facets exhibit low surface energy, thus facilitating the contraction of liquid droplets, while the polar facets exhibit high surface energy and facilitate liquid spreading (Ghannam et al., 2019; Mardosaitė et al., 2021). We have previously characterized our CVD-grown ZnO NWs using X-ray diffraction and showed that they exhibit predominantly non-polar facet termination (Alameri et al., 2017a), thus suggesting that our samples could have tendencies towards hydrophobicity. The observed lower values of the contact angle for the SWCNTs can be attributed to the lower surface coverage and flat surface morphology. Moreover, the areas of the SiO_2/Si surface that were not covered by SWCNTs contributed to more hydrophilic manifestations as compared to the densely packed ZnO NWs samples.

The representative AFM image (Figure 2D) obtained on SiO_2/Si substrates reveals the diameter distribution of SWCNTs within the 1.7–2.2 nm range, as depicted in three topographic line profiles (Figure 2E). The SWCNTs diameters are denoted by stars in the line profiles, while other discernible peaks correspond to nanocatalyst particles that have aggregated during the growth process. These observations corroborate the predominantly single-walled composition of the SWCNTs. In Figure 2F, a 3D-AFM image acquired from another sample and the line profile shown below showed a sub-nanometer roughness of 0.62 nm root mean square (RMS) value. The diameter distribution also confirms the typical range from 1.2 to 2.25 nm for SWCNTs. Notably, all measured diameters of the SWCNTs remained consistent, affirming the uniformity of SWCNTs across different samples. Note that the AFM analysis also revealed the presence of the aggregated larger nano-catalyst particles on the SWCNTs samples, which were likely participating in a nucleation process of the ZnO NWs in the subsequent heterostructure formation. As a result, the average diameter of ZnO NWs grown on top of the SWCNTs within the heterostructure were larger, as compared to ZnO NWs sample grown directly on SiO_2/Si substrates, as seen in the SEM images in Supplementary Figure S1.

The quality of the nanomaterials was assessed by Raman spectroscopy (Figure 2G). SWCNTs have unique Raman signals in the radial breathing mode (RBM) (~100–350 cm^{-1}), the D-band (~1,350 cm^{-1}), and the G-band (~1,580 cm^{-1}). It was found from the RBM Raman shifts that the diameters of the SWCNTs were between 1.7 and 2.3 nm, which also confirms our direct AFM measurement results (Jorio et al., 2001) In addition, Raman data show the full width at half maximum (FWHM) of the G-band, of the SWCNTs was in the range of 18–21 cm^{-1} for both samples, namely, SWCNTs and ZnO NWs/SWCNTs, indicative of high crystallinity. At the same time the G- and D-band intensity ratio (I_G/I_D) was found to be in the range of 10–25 (Alameri et al., 2017b). These results are evidentiary of the high quality of the SWCNTs. It also verifies that SWCNTs are not being compromised (no defects were created) during the growth of the ZnO NWs on top of the SWCNTs in the process of the heterostructure formation. ZnO NWs also display characteristic Raman spectra, which respectively allow us to evaluate their quality and crystallinity. ZnO NWs have wurtzite crystal structure (Geng et al., 2004; Zhu et al., 2012; Al-Asadi et al., 2017). The lattice optical phonon with A_1, E_1, and E_2 being most Raman active. E_2 mode shows the crystallinity level of as-grown ZnO NWs. Raman spectra of representative positions show high-intensity modes for E_2^{low} and E_2^{high} (98.7 and 436.9 cm^{-1}), which are associated with Zn and O_2 sublattices, respectively. The FWHM of the most intense E_2^{high} peak in the Raman spectra of ZnO NWs and ZnO NWs/SWCNTs is ~7.6 cm^{-1}, indicating a high level of crystallinity in both cases. Raman spectra collected from the heterostructure samples show SWCNTs and ZnO NWs characteristic main peaks and demonstrate preserved integrity of both materials.

3.2 Cell spreading and viability on SWCNTs, ZnO NWs, and ZnO NWs/SWCNTs

To study the effects of SWCNTs, ZnO NWs, and ZnO NWs/SWCNTs on cell area, shape factor, and viability, U87 glioblastoma cells and NIH 3T3 fibroblast cells were used. The cells were chosen as the model cells for a commonly used cancer cell type (U87 cells) and a commonly used normal cell type (NIH 3T3) to capture possible differing effects of the nanomaterials on normal vs. cancer cells. U87 glioblastoma cells were chosen for this study due to previous studies indicating ZnO nanostructure suppression of glioblastoma tumor cell viability (Wahab et al., 2011; Zhu et al., 2012). NIH 3T3 fibroblast cells have also been commonly used for *in vitro* toxicity studies, due to being the most abundant cell types within all connective tissues (Boncler et al., 2019).

Cell spreading and circularity as a function of nanomaterial composition were similar for both cell types (Figure 3). For both U87 and NIH 3T3 cells, we noted decrease in cell spreading and increase in cell circularity for cells on the ZnO NW and the ZnO NWs/SWCNTs heterostructures compared to all other conditions, possibly indicating ZnO cytotoxicity or inability to support cell spreading. There was no significant difference between cell spreading or circularity on the ZnO NWs or ZnO NWs/SWCNTs, indicating that the effect of ZnO NWs was dominant. This was not surprising, since the ZnO NWs were grown on top of the SWCNTs, so it is possible that cells were only able to sense the ZnO NWs due to direct contact mostly with the ZnO NWs layer. For both cell types seeded on ZnO NWs and ZnO NWs/SWCNTs we observed a significant ~2-fold decrease in cell area and ~2-fold increase in circularity as compared to cells on SWCTNs or control samples/chips. For both cell types, spreading area was highest on the SWCNTs, and it was significantly higher than the controls for U87 cells. This was also expected as we and others have previously shown that SWCNTs facilitate cell spreading (Imaninezhad et al., 2018).

Live/dead staining for U87 and NIH 3T3 showed more live cells with elongated morphologies on SiO_2/Sicontrols and SWCNTs compared to ZnO NWs or ZnO NWs/SWCNTs heterostructures (Figure 4). The higher cell viability for cells on control SiO_2/Si control samples/chips and SWCNTs, compared to ZnO NWs and ZnO NWs/SWCNTs corroborated the cell spreading data, indicating that decreased cell spreading could be due to decreased cell viability. For both cell types, there was no significant difference between cell viability on SiO_2/Si chips and SWCNTs, with viability being >80% for all conditions. On ZnO NWs and ZnO NWs/SWCNTs, U87 cell viability decreased to ~25%, and for NIH 3T3 cells it decreased even further to ~6%.

3.3 Cell filopodia on SWCNTs, ZnO NWs, and ZnO NWs/SWCNTs

Upon closer observation of the cells through SEM imaging, we were able to qualitatively observe cell filopodia on each nanostructure, albeit with some pronounced differences between conditions. For U87 cells (Figure 5A), cells extended long and dense filopodia on the SiO_2/Si controls and SWCNTs, with an evident decrease in filopodia length and density for cells on ZnO NWs and ZnO NWs/SWCNTs. Similar observations were made for NIH 3T3 cells, where cells on the SWCNTs seemed to have denser and longer filopodia than cells on the control SiO_2/Si, and both were higher than the ZnO NWs and ZnO NWs/SWCNTs (Figure 5B). By quantifying the lengths of filopodia from cells for

10.3389/frcrb.2024.1400664

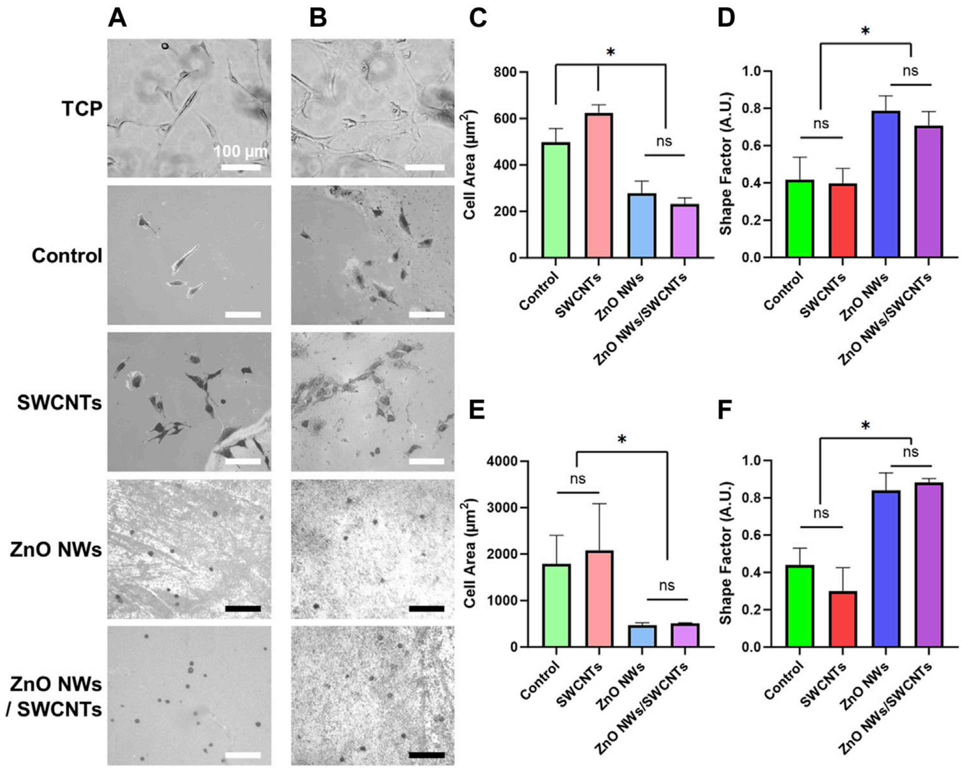

FIGURE 3
NIH 3T3 and U87 cell area and shape factor on TCP, SiO_2/Si control/reference samples (Control), SWCNTs, ZnO NWs, and ZnO NWs/SWCNTs at 24 h of culture. **(A)** Phase contrast microscopy images of NIH 3T3 cells and **(B)** U87 cells on each nanomaterial as well as SiO_2/Si control samples/chips (Control) without nanomaterials and tissue culture polystyrene (TCP). Scale bar = 100 µm. **(C)** Cell area and **(D)** Shape factor of NIH 3T3 cells as a function of nanomaterial composition. **(E)** Cell area and **(F)** Shape factor for U87 cells as a function of nanomaterial composition. * designates significant differences (n = 6 for NIH 3T3, n = 3 for U87, $p < 0.05$).

each condition, it was found that cells on SWCNTs generally had longer filopodia than all other conditions. The most noticeable difference was the increase of filopodia lengths of NIH 3T3 cells on SWCNT, compared to the control SiO_2/Si (Figure 5C). NIH 3T3 filopodia on SWCNTs were an average of 24.7 µm, which was much larger than filopodia averages of 2.0 and 3.3 µm on ZnO NWs, and ZnO NWs/SWCNTs, respectively. Note that due to vastly divergent dimensions, it was challenging to show high resolution images for both cells and cell filopodia and the underlying SWCNTs; hence, separate images with the focus adjusted to show the underlying SWCNTs is shown in Supplementary Figure S3. Lastly, filopodia lengths were lowest for ZnO NWs and ZnO NWs/SWCNTs for both cell types.

Though cell area decreased, and shape factor increased on nanomaterials containing ZnO NWs, for both NIH 3T3 and U87 cells, there was still filopodia extensions on the ZnO NWs. Upon closer inspection, NIH 3T3 cells in areas of varying ZnO NWs density had different filopodia numbers and length. On areas of highest ZnO NWs density, there were short but numerous filopodia extending from the cells. On areas of lesser ZnO NWs density, the cells had fewer filopodia, and decreased cell area. For areas of the least ZnO NWs density, the cells did not seem to extend filopodia and had a round morphology (Supplementary Figure S4). This data suggests that though NIH 3T3 fibroblasts and U87 glioma cells show decreased proliferation and cell area on ZnO NWs, they still can interact with the ZnO NWs, perhaps in a density dependent manner.

3.4 ZnO NWs conditioned media effect on NIH 3T3 and U87 cell spreading and viability

Due to the decreased cell area and increased shape factor, as well as decreased viability for ZnO NWs and heterostructures, we sought to further study ZnO NWs' toxicity to U87 and NIH 3T3 cells by exposing them to ZnO NW conditioned media. We characterized the conditioned media via DLS and compared it to non-conditioned media. DLS analysis of the ZnO NWs conditioned media showed that particle sizes in the media were similar to the unconditioned media (Supplementary Figure S5), suggesting that there are no agglomerated or nano-or micro-size particles from the ZnO NWs. This data implies that the toxic effect from the ZnO NWs conditioned media should be from soluble/degradation compounds, such as ions, released in the media, rather than NWs structures or particulates being released from the ZnO NWs/SiO_2/Si samples.

To test the effect of ZnO NWs releasates on cells, we first cultured cells on TCP and then exposed them to ZnO NWs conditioned or non-conditioned media for 48 h (Figure 6). After exposing U87 cells to ZnO NWs conditioned media, cell area

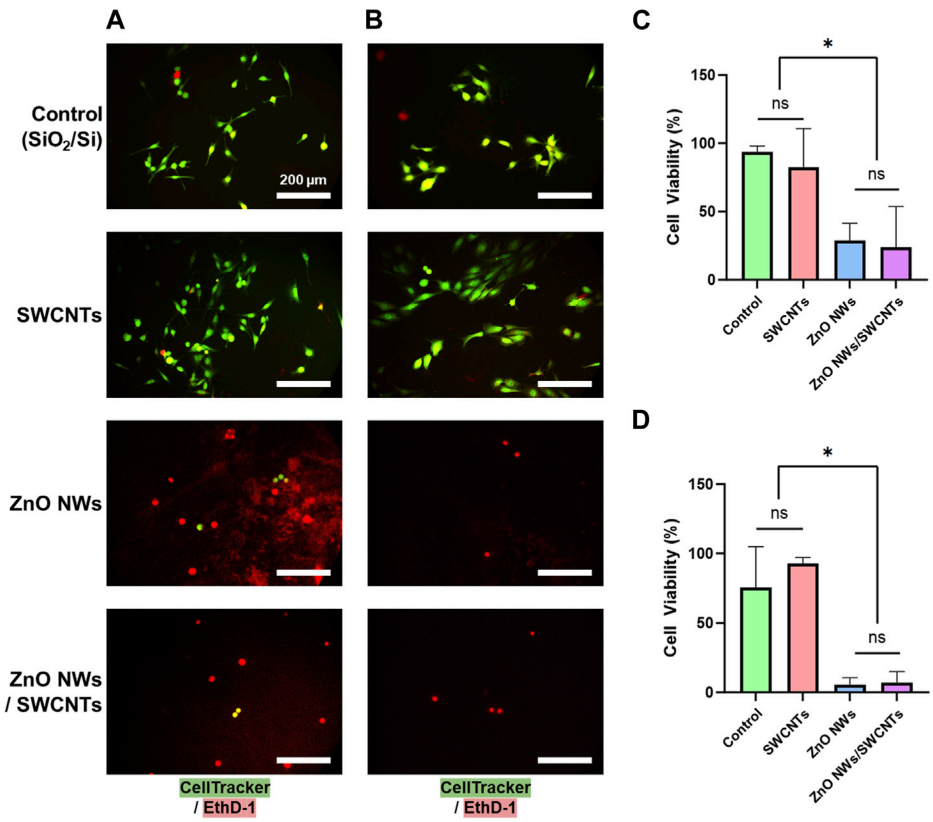

FIGURE 4
NIH 3T3 and U87 cell viability on SiO_2/Si reference/control samples (Control) and nanomaterial; SWCNTs, ZnO NWs, and ZnO NWs/SWCNTs. **(A)** Fluorescence microscopy images of U87 cells on nanomaterials. **(B)** Fluorescence microscopy images of NIH 3T3 cells on nanomaterials. Green = Calcein AM (stains live cells), Red = EthD-1 (stains nuclei of dead cells). Scale bar = 200 µm. **(C)** U87 cell and **(D)** NIH 3T3 cell viability on each nanomaterial as calculated from live/dead staining. * designates significant differences (n = 3, $p < 0.05$).

noticeably decreased after 24 and 48 h of exposure (Figures 6A, B). The shape factor of U87 cells at 48 h with non-conditioned growth media was an average of 0.30 ± 0.05, while U87 cells at 48 h exposure to conditioned media was much higher, at 0.70 ± 0.08, indicative of a round morphology (Figure 6C). NIH 3T3 cells also significantly decreased in cell area with exposure to conditioned media after 48 h (Figure 6D). Cells with non-conditioned media on TCP had an average area of 1,100.1 ± 103.2 µm^2, while cells on TCP exposed to conditioned media had an average cell area of 379.0 ± 46.9 µm^2 (Figure 6E). As seen in Figure 6F, the shape factor had also decreased at 24 and 48 h. At 48 h, the shape factor of NIH 3T3 cells on TCP with growth media was an average of 0.34 ± 0.06, while cells exposed to conditioned media had an increased shape factor to 0.73 ± 0.05 (Figure 6F).

Overall, both cell types experienced similar changes in spreading and morphology when exposed to ZnO NWs conditioned media for 48 h. Compared to non-conditioned media, we noted a significant decrease in cell spreading area and a significant increase in shape factor for both U87 and NIH 3T3 cells, showing that while cells were well spread and elongated in non-conditioned media, they were round in conditioned media indicating toxicity.

In addition to cultured cells on TCP, we also examined the effect of ZnO NWs conditioned media towards cells cultured on the SiO_2/Si control samples and on the SWCNTs samples to determine whether those substrates provided rescue towards cell viability and spreading (Figure 7). Corroborating TCP results at 48 h of exposure, U87 and NIH 3T3 cells showed significantly decreased cell areas and increased shape factor (i.e., round morphology) compared to unconditioned media for both cells on SiO_2/Si controls and on SWCNTs (Figures 7A, C). Also, qualitative evaluation showed a substantially decreased cell presence for both cell types when exposed to ZnO NWs conditioned media independent of the growth substrate, indicative of toxicity.

We further used live/dead staining of U87 and NIH 3T3 cells to investigate cell viability. U87 cells visually decreased in cell number and had a higher ratio of EthD-1-stained dead cells when exposed to ZnO NW conditioned media (Figures 7A, C). U87 cells on the SiO_2/Si controls and on the SWCNTs/SiO_2/Si samples had high viability of 88.1% ± 4.1% and 91.4% ± 5.5%, respectively. U87 cells on the controls and on the SWCNTs samples showed decreased cell viability when exposed to conditioned media, by 16.2-fold and 4.3, respectively. The cell viability on the control sample was 81.6% ± 11.6% and on SWCNTs it was 96.6% ± 1.8% (Figure 7B). This pattern was also seen for NIH 3T3 cells, where cell viability on the control conditioned media, cell viability decreased 3.6-fold and 3.2-fold for cells on SiO_2/Si controls and SWCNTs samples, respectively (Figure 7D). Similarly to U87 and NIH 3T3 cells cultured on SiO_2/Si controls and the SWCNTs

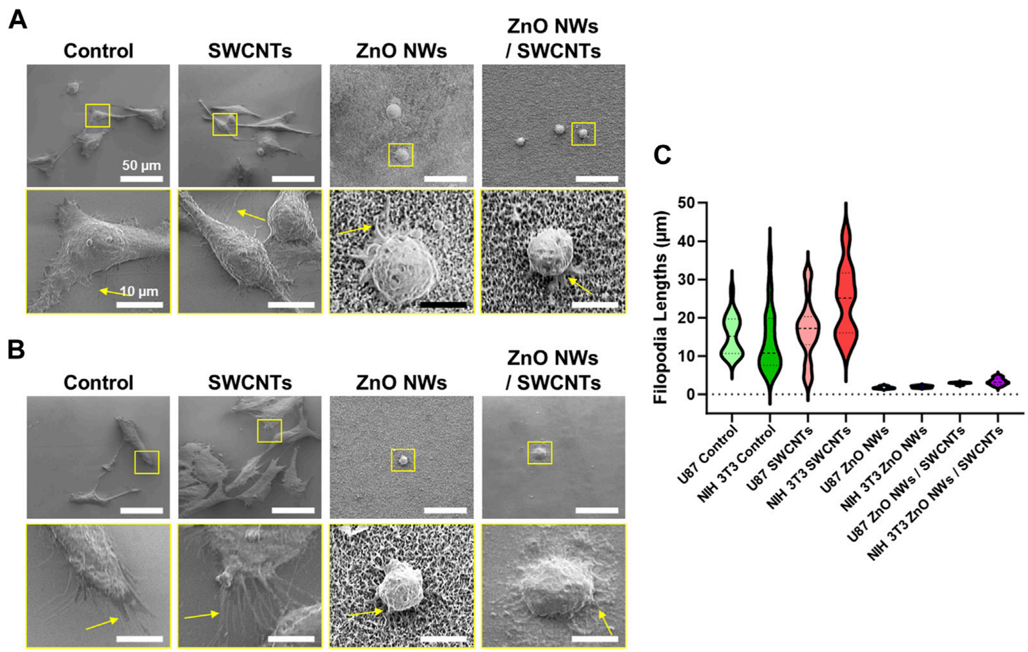

FIGURE 5
Cell filopodia characterization on SiO_2/Si reference/control samples (Control), as well SWCNTs, ZnO NWs, and ZnO NWs/SWCNTs. Cells were cultured for 24 h on each substrate. **(A)** SEM images of U87 cells on each nanomaterial, with the corresponding zoomed-in insets to observe the filopodia. Scale = 50 µm and 10 µm, respectively. **(B)** NIH 3T3 cells on top of each nanomaterial, with zoomed in insets to observe the filopodia. Scale = 50 µm. **(C)** Filopodia lengths for each condition.

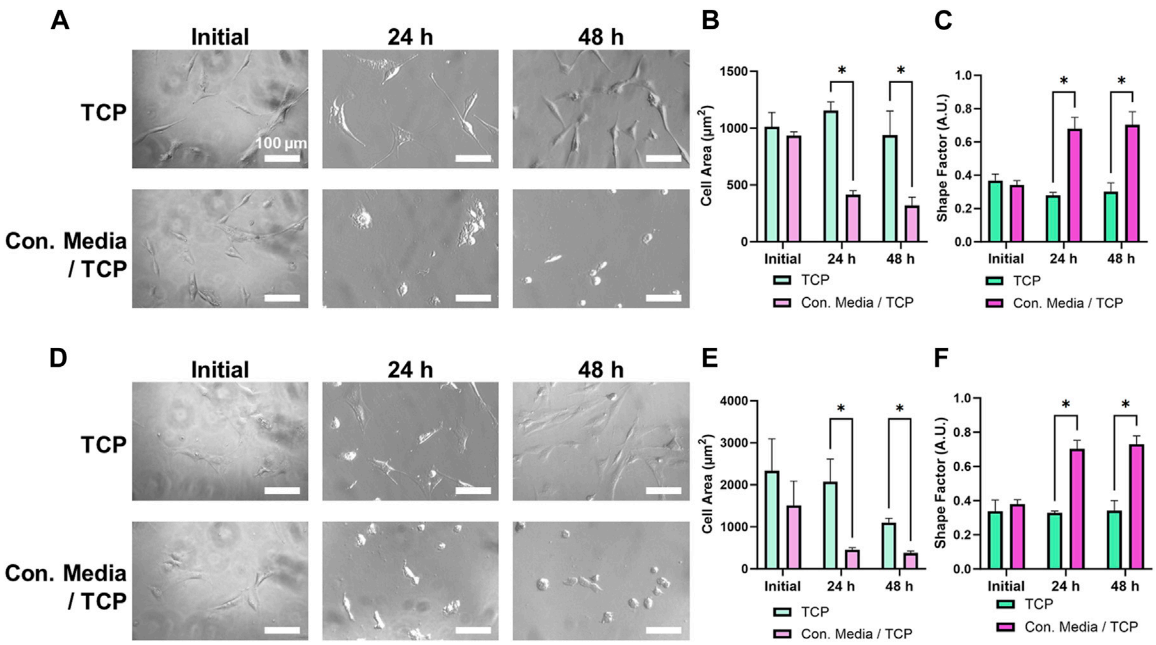

FIGURE 6
U87 and NIH 3T3 cells cultured on TCP for 24 h, then exposed to conditioned media for 48 h. **(A)** Phase contrast images of U87 cells on TCP exposed to non-conditioned or conditioned media. Scale bar = 100 µm. U87 cell area **(B)** and shape factor **(C)** as a function of media conditioning. **(D)** Phase contrast images of NIH 3T3 cells on TCP exposed to non-conditioned or conditioned media. Scale bar = 100 µm. NIH 3T3 cell area **(E)** and shape factor **(F)** as a function of media conditioning. * designates significant differences (n = 3, $p < 0.05$).

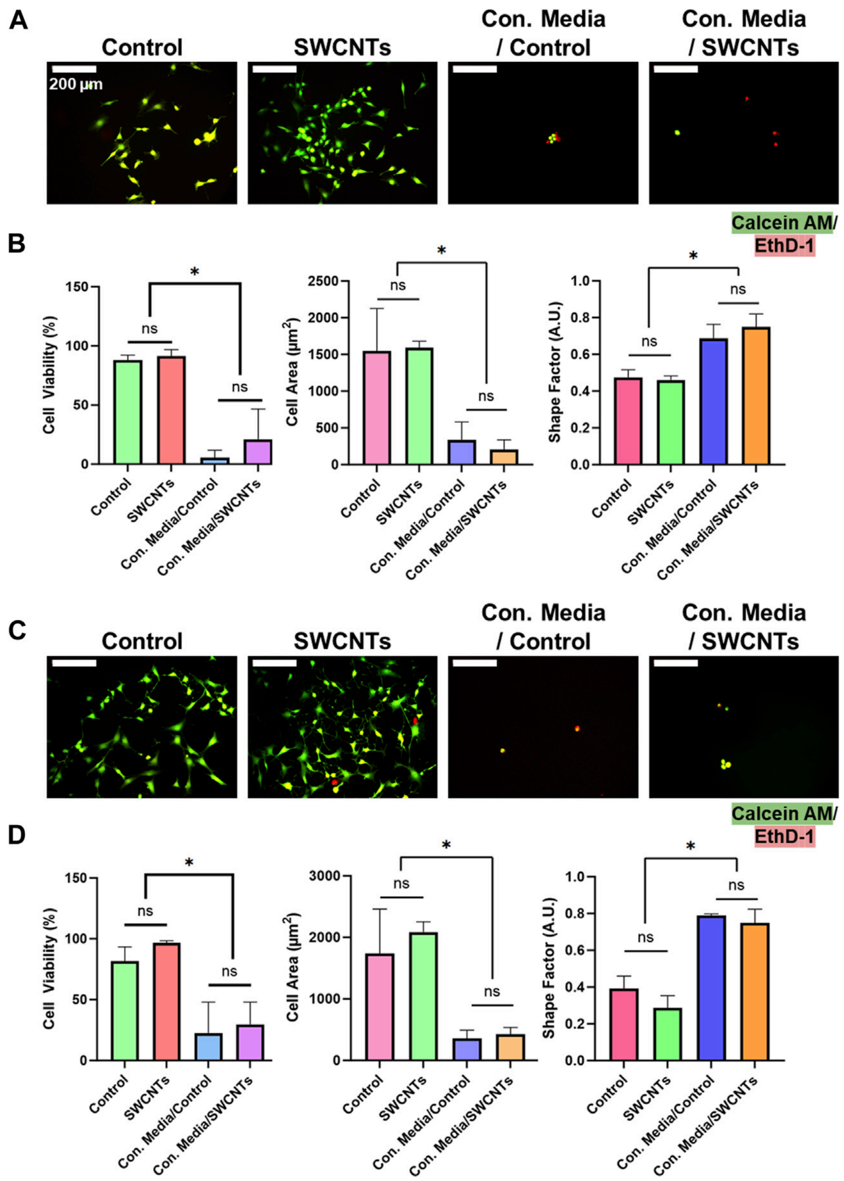

FIGURE 7
NIH 3T3 and U87 cell viability, area, and shape factor on SiO_2/Si control samples (Control) and SWCNTs, when exposed to conditioned media for 48 h. **(A)** Fluorescence microscopy images of U87 cells on nanomaterials. Green = Calcein AM (stains live cells), Red = EthD-1 (stains nuclei of dead cells). Scale bar = 200 μm. **(B)** U87 cell viability, area and shape factor when exposed to ZnO NWs conditioned media on Control and SWCNTs. **(C)** Fluorescence microscopy images of NIH 3T3 cells on nanomaterials. Scale bar = 200 μm. **(D)** NIH 3T3 cell viability, area and shape factor when exposed to ZnO NWs conditioned media on the SWCNTs and Control samples. * designates significant differences ($n = 3$, $p < 0.05$).

samples, cells that were found in the TCP wells next to the substrates with nanomaterials on them, showed reduced viability when exposed to ZnO NWs conditioned media (Supplementary Figure S6). This result indicated that any loss in cell viability was not due to the underlying substrate (the SiO_2/Si or the SWCNTs), but only the conditioned media.

Previous studies (Li et al., 2011; Liao et al., 2020) have indicated that the cytotoxicity of ZnO nanomaterials may be attributed to the dissolution of Zn^{2+} from the materials, potentially leading to adverse effects upon cellular uptake. To investigate this, the Zn^{2+} concentration in the cell media was estimated using average length/diameter and the surface coverage data provided by high resolution SEM images. Supplementary Table S1 shows the calculated concentration of Zn^{2+} ions to be in the range of 2.3–10.2 μg/mL for the ZnO NWs samples soaked in RPMI compared to a similar range of 2.8–10.2 μg/mL when soaked in DMEM, hence, there is not a significant difference between the two media types used for cell culture. However, for the ZnO NWs/SWCNTs heterostructure samples soaked in RPMI, concentration of Zn^{2+} ions ranged from 1.3–4.6 μg/mL, and for the heterostructures soaked in DMEM, Zn^{2+} ion concentration ranged from 1.5–5.2 μg/mL Although there appears to be no difference in dissolution across the 2 cell medias, there is a clear lower dissolution in the case of

ZnO NWs/SWCNTs heterostructure samples as compared to the solely ZnO NWs.

4 Discussion

In this study we used CVD synthesis to fabricate high quality nanomaterials such as SWCNTs, ZnO NWs and the heterostructures ZnO NWs/SWCNTs on SiO_2/Si substrates with controlled morphology (Figures 1, 2) to examine behaviors of two different cell lines, namely, U87 glioblastoma and NIH 3T3 fibroblast cells, chosen to represent both a cancerous and a normal cell type. While the 2 cell types are representative, a more comprehensive cell panel could be tested in the future to broaden our understanding of cell-nanomaterial interactions. One-dimensional nanomaterial prepared either in lateral monolayer networks (such as SWCNTs) or vertically oriented forests (such as ZnO NWs) have unique biomedical relevance. Heterostructures made from these one-dimensional nanomaterials can add additional versatility in creating compound platforms with dual purposes in biomedical applications. The goal was to study cell viability, spreading, and morphology on top of the SWCNTs, ZnO NWs, and their heterostructure to gain knowledge on the suitability of the nanomaterials as cell substrates or testbeds. While there are multitude of studies of cell behaviors on SWCNTs including by our team, there have been fewer studies involving highly crystalline ZnO NWs. On the other hand, heterostructures of ZnO NWs/SWCNTs have not been explored. Additionally, there are conflicting reports on the toxicity of ZnO. For example, ZnO NWs have been shown as a promising neuronal substrate (Onesto et al., 2019), while ZnO nanorods have been shown to resist cell adhesion (Lee et al., 2008), and yet others have shown that ZnO in the form of a flat film, nanorods or nanowires is toxic to cells (Ghaffari et al., 2019).

In our study we showed that cells cultured onto ZnO NWs and ZnO NWs/SWCNTs decreased in cell area and became more circular, which also corresponded to a significant decrease in cell viability (Figures 3, 4). Our results corroborate a study that observed that NIH 3T3 cells do not have initial spreading on ZnO NWs, nor filopodia formation, due to the inability of cells to adhere to the nanowire substrates and the effects of substrate surface on cell growth (Lee et al., 2008). Another study found that the presence of ZnO NWs, along with toxic by-products after longer periods of culture, may slow down initial cell adhesion and growth rate (Gaetani et al., 2022).

For cells on SWCNTs, we noted larger cell spreading and smaller shape factors. Cell spreading on the SWCNTs is dependent on cell integrin binding facilitated by adsorption of serum and cell-secreted adhesive proteins onto the SWCNTs, as shown by us previously (Imaninezhad et al., 2018). Furthermore, integrin attachment enhances the signaling of growth factors, to which then FAK acts as a downstream target. FAK plays an important role in cell migration, adhesion and regulation for U87 and NIH 3T3 cells (Riemenschneider et al., 2005). Note that while some literature, where nano-powder SWCNTs were used, suggests that SWCNTs are suppressive towards U87 glioblastoma cells (Minchenko et al., 2016), this was not the case in this study as discussed above. This may be due to the fact that cells were grown on top of the CVD-synthesized SWCNTs networks which are attached to the growth substates, and not in media with dispersed SWCNTs powders, as reported in other studies. Here, the as-grown SWCNTs were attached (prepared directly) onto the SiO_2/Si substrate, hence not available for cell endocytosis due to their strong van der Waals attraction to the SiO_2/Si growth substrate (Dai et al., 2001).

On further examining cell morphology, we noted that NIH 3T3 filopodia on SWCNTs were an average of 24.7 μm, which was significantly larger than filopodia averages of 2.0 μm and 3.3 μm on ZnO NWs, and ZnO NWs/SWCNTs, respectively (Figure 5). Fibroblasts also favor probing rigid substrates with filopodia extensions before migration (Wong et al., 2014), hence the larger filopodia length on the SWCNTs was indicative of a more favorable substrate for cell adhesion and migration compared to ZnO NWs. This could also be due to a flatter (nanotextured) surface of the SWCNTs networks-bed as compared to a more 'spiky' ZnO NWs forest interfaces. While both cell types exhibited longer filopodia on the SWCNTs compared to the other nanomaterials, NIH 3T3 fibroblasts had overall more elongated morphology than the U87 cells, which had a more epithelial-like shape (Supplementary Figure S3).

We then aimed to determine whether the lower cell viability and spreading on the ZnO NWs and ZnO NWs/SWCNTs heterostructure was due to the vertical and 'spiky' morphology of the ZnO NWs or due to NWs degradation products. Others have previously shown that cells, specifically neural-like PC12 cells, could extend filopodia, spread and retain high cell viability on vertical collagen-coated ZnO NWs (Ciofani et al., 2012). Beyond ZnO, significant previous research on vertical NW arrays has shown not only that cells can adhere and grow on vertical arrays, but that NW density and diameter can be used to control cell adhesion, morphology, motility, and differentiation (Qi et al., 2009; Persson et al., 2015; Li et al., 2018). For example, breast cancer cells showed an overall lower cell areas and larger focal adhesions at the cell edges for lower diameter NWs compared to higher spreading areas and punctate focal adhesions on larger diameter NWs (Li et al., 2018). Further, increased NW density was shown to increase motility of fibroblasts, but a reduced cell proliferation was noted irrespective of NW density (Persson et al., 2015). Another study of human hepatic and hepatoma cell lines showed that vertical NWs supported cell adhesion and growth and enhanced cell-substrate adhesion force, but restricted cell spreading. The authors attributed the lower cell spreading area on the spiky morphology of the nanowires, where cells were able to extend filopodia and form focal adhesions initially, but were not able to reach out at a distance from their first contact point (Qi et al., 2009).

Hence, we hypothesized that the spiky morphology might be responsible for the lower cell spreading, but it should not be responsible for the lower cell viability. To test for that we used ZnO NW-conditioned media (ZnO NWs soaked in media for up to 48 h) on cells seeded on TCP only or on TCP in the presence of SWCNTs (Figures 6, 7). ZnO NWs have been reported to initiate degradation in ~30 min, which results in the release Zn^{2+} ions (Milano et al., 2018). With the released Zn^{2+} ions, the ZnO NWs may generate reactive oxygen species (ROS). In turn, these compounds may cause cytotoxic cellular effects that include intracellular calcium flux, mitochondrial depolarization, and plasma membrane leakage (George et al., 2010). Therefore, decreased cell area with ZnO NWs conditioned media may be attributed to the cytotoxic effects from soluble compounds present in the media, which is what our data indicated. Another study on ZnO NWs conditioned media found that cytotoxicity was occurring due to accumulation of by-products from ZnO NWs with 3 days of incubation in 1 mL of medium per sample area of 1 cm^2. In addition to a decrease in cell survival, cells on ZnO NWs retained round morphology, which pointed towards poor cell adhesion (Gaetani et al., 2022). This may also explain the decrease in cell counts for cells in conditioned media and on structures including ZnO NWs, since cells may have been washed off during handling for fixation and live/dead staining.

From the dissolution analysis, it was determined that regardless of whether the medium was RPMI or DMEM, the medium containing the ZnO NWs samples had an approximate Zn^{2+} concentration ranging from 2.3 μg/mL to 10.2 μg/mL (as shown in Supplementary Table S1). Our results seem to be in line with the previously reported studies, which state that at similar concentrations the medium showed to be toxic (Liao et al., 2020). Previous studies have also shown that Zn^{2+} ions released from ZnO structures were responsible for PC12 neural-like cell death, regardless of whether the ZnO were nanorods, nanowires or solid thin films (Ghaffari et al., 2019). The medium containing the ZnO NWs/SWCNTs heterostructures had slightly lower Zn^{2+} ion concentration ranging from 1.3 μg/mL to 5.2 μg/mL. The lower dissolution could potentially be attributed to the enhanced interaction between the ZnO NWs with the SWCNTs networks due to a direct synthesis of one material on top of another. On the other hand, the presence of the SWCNTs could also effectively increase the hydrophobic surface area, thus decreasing the ZnO -solvent interactions.

Overall, our studies indicated that ZnO NWs were not conducive to cell growth for the cell types and growth conditions tested here. This was not due to the inability of cells to adhere to the ZnO NWs or due to their vertically oriented 'spiky' surface topography. In fact, cells were able to extend filopodia on NWs even when they still decreased in spreading area. The filopodia extensions despite the 'spiky' morphology were not surprising as other have shown that cells, specifically neuronal cells, were able to form neuronal networks when grown on ZnO NWs over 7 days (Onesto et al., 2019). The decrease in cell area and cell viability was instead attributed to the release of Zn^{2+} from the nanostructures. While cells were able to spread and retain high viability on SWCNTs as expected, SWCNTs were not able to 'rescue' cell growth in the heterostructures as we had hoped despite decreasing the Zn^{2+} concentration. Note that one limitation to the study was that we used live-dead staining to assess cell viability, so it is possible that some cells were washed off the surface during staining due to weak adhesion (e.g., rounded cells, which might otherwise be alive could not be stained) or due to necrosis (hence dead cells were not stained). Despite that, the decrease in cell spreading and cell presence clearly pointed to the toxic effect of the ZnO NWs on the cells. Despite previous reports on the selective negative effect of ZnO on cancer cells compared to normal cells, we observed similar toxicity for both cell types, possibly because of the high dose of Zn^{2+} ions released in the media due to the high density and volume of the ZnO NWs on which the cells were seeded. Previous studies have shown that the toxicity of ZnO is concentration dependent. For Zn^{2+} concentrations of ~2–10 μg/mL, it was generally being found to be cytotoxic (Liao et al., 2020). Even for the heterostructures which contained a lower Zn^{2+} concentration of ~1–5 μg/mL, this was still found to be in the cytotoxic range (Alameri et al., 2017b). Future investigations focusing on varying densities of ZnO NWs and SWCNTs which could be modulated by growth parameters would be interesting to pursue.

It is important to note that we determined the extracellular Zn^{2+} ions released by ZnO NWs through measuring the ZnO NWs dissolution. Despite finding that the percent dissolution was similar in both DMEM and RPMI media and that the ZnO NWs/SWCNTs samples had less dissolution than ZnO NWs samples, there could be potential interactions with various components in the cell media that could affect cellular uptake of these ions. For example, RPMI has a lower amino acid concentration (~1,000 mg/L) than DMEM (~1,600 mg/L) which has been shown to decrease Zn^{2+} toxicity as the amino acids can complex and effectively remove Zn^{2+}, which would not be detected via our Zn^{2+} concentration determination method (Li et al., 2011). However, with many competing factors present in cell media, it can be hard to predict what the overall effect would be (Li et al., 2011; Li et al., 2013). In future studies, using a fluorescent sensing method to measure the intracellular labile Zn^{2+} can be beneficial in discerning more of the cell media effect (Pratt et al., 2021). Furthermore, measuring the rate of cellular uptake of Zn^{2+} will give more insight into the mechanism behind cell death and whether the morphology of the underlying nanomaterials plays a role in the cellular uptake of these ions.

Altogether, our results have several important implications. They suggest that the surface topography of both SWCNTs (horizontal networks) and ZnO NWs structures (vertically oriented forests) are amenable for use as cell substrates in biomedical applications. The use of SWCNTs and ZnO in biomedical applications needs further investigation and possibly consideration of other nanomaterials such as two-dimensional (2D) graphene (Gr) in combination with patterned 2D ZnO nanostructures which could offer an additional level of local control in preparation of heterostructures and predetermined coverage and amount of ZnO NWs interacting with cells, while as the same time offering an ability to observe selective and localized cell behaviors on patterned vs. unpatented surfaces and substrates. Further investigations should also include a variety of cell types to provide a more comprehensive understanding of nanomaterial-cell interactions as a function of cell type.

Our results indicate that SWCNTs, ZnO NWs, and ZnO NWs/SWCNTs heterostructures could be valuable substrates in future biomedical applications. For example, if SWCNTs are prepared to contain high percentages of CVD grown metallic SWCNTs or multiwalled carbon nanotubes (MWCNTs), which are also predominately metallic, thus having higher thermal and electrical conductivity, then biomedical uses of such systems in heterostructure form could expand its further scope. In particular, the applications could involve effective thermal stimulation of cells or embedding heterostructures into hydrogel matrices or other types of biomaterials used as drug delivery vehicles. Our study indicated that the presence of carbon nanotubes in the heterostructures affected the rate of dissolution of ZnO, therefore further studies using other forms of carbon, such as 2D graphene or nanodiamond films in the heterostructure assemblies could provide new insights into the nature of carbon - zinc oxide interaction in the cell media environments.

5 Conclusion

Here we used chemical vapor deposition to fabricate substrates with coatings of semiconducting SWCNTs, ZnO NWs and ZnO NWs/SWCNTs heterostructures and investigated their effect on cell viability and spreading for representative normal and cancer cells seeded on top of the nanomaterials. We first confirmed the high quality of the grown nanomaterials by several different methods, including SEM, AFM and Raman spectroscopy. We found that the nanomaterials containing ZnO NWs decreased viability and cell spreading for both U87 and NIH 3T3 fibroblast cell types, even though cells were able to extend filopodia on the ZnO NWs. Further studies of cell viability in ZnO NWs conditioned media, showed that the apparent ZnO NWs toxicity was due to dissolution by-products, such as Zn^{2+} ions released from the nanomaterials, rather than the ZnO NWs surface topography. Our results may inform future uses of SWCNTs, ZnO NWs, and ZnO NWs/SWCNTs heterostructures in biomedical applications.

Data availability statement

The original contributions presented in the study are included in the article/Supplementary Material, further inquiries can be directed to the corresponding authors.

Ethics statement

Ethical approval was not required for the studies on humans in accordance with the local legislation and institutional requirements because only commercially available established cell lines were used.

Author contributions

EL: Formal Analysis, Investigation, Validation, Visualization, Writing–original draft. BA: Formal Analysis, Investigation, Validation, Visualization, Writing–original draft, Writing–review and editing. YK: Formal Analysis, Validation, Visualization, Writing–original draft, Writing–review and editing. ML: Investigation, Validation, Visualization, Writing–review and editing. PJ: Formal Analysis, Writing–review and editing. SZ: Conceptualization, Formal Analysis, Funding acquisition, Methodology, Project administration, Writing–review and editing. IK: Conceptualization, Formal Analysis, Funding acquisition, Methodology, Project administration, Supervision, Writing–review and editing.

Funding

The author(s) declare that financial support was received for the research, authorship, and/or publication of this article. This research was partially supported through a President's Research Fund awarded to IK and SZ from Saint Louis University. IK also acknowledges support of Billiken Boost Program sponsored and funded by the Provost's Office in collaboration with the Faculty Gender Equity Committee, Faculty Fellow for Equity Issues, and the Division of Diversity and Innovative Community Engagement. The research was also partially funded through two ILEX funds awarded to EL and ML from the Honors Program at Saint Louis University.

Acknowledgments

The authors acknowledge Dr. Alaina Baker-Nigh for access to and assistance with an upright fluorescent microscope for cell imaging studies.

Conflict of interest

The authors declare that the research was conducted in the absence of any commercial or financial relationships that could be construed as a potential conflict of interest.

The author(s) declared that they were an editorial board member of Frontiers, at the time of submission. This had no impact on the peer review process and the final decision.

Publisher's note

Supplementary material

The Supplementary Material for this article can be found online at: https://www.frontiersin.org/articles/10.3389/frcrb.2024.1400664/full#supplementary-material

References

Alameri, D., Ocola, L. E., and Kuljanshvili, I. (2017a). Controlled selective CVD growth of ZnO nanowires enabled by mask-free fabrication approach using aqueous Fe catalytic inks. *Adv. Mater. Interfaces* 4, 1700950. doi:10.1002/ADMI.201700950

Alameri, D., Ocola, L. E., and Kuljanshvili, I. (2017b). Controlled selective CVD growth of ZnO nanowires enabled by mask-free fabrication approach using aqueous Fe catalytic inks. *Adv. Mater. Interfaces* 4, 1700950. doi:10.1002/admi.201700950

Al-Asadi, A. S., Henley, L. A., Wasala, M., Muchharla, B., Perea-Lopez, N., Carozo, V., et al. (2017). Aligned carbon nanotube/zinc oxide nanowire hybrids as high performance electrodes for supercapacitor applications. *J. Appl. Phys.* 121, 121. doi:10.1063/1.4979098

Bacakova, L., Grausova, L., Vacik, J., Fraczek, A., Blazewicz, S., Kromka, A., et al. (2007). Improved adhesion and growth of human osteoblast-like MG 63 cells on biomaterials modified with carbon nanoparticles. *Diam. Relat. Mater.* 16, 2133–2140. doi:10.1016/j.diamond.2007.07.015

Bisht, G., and Rayamajhi, S. (2016). ZnO nanoparticles: a promising anticancer agent. *Nanobiomedicine (Rij)* 3, 9. doi:10.5772/63437

Boncler, M., Lukasiak, M., Dastych, J., Golanski, J., and Watala, C. (2019). Differentiated mitochondrial function in mouse 3T3 fibroblasts and human epithelial or endothelial cells in response to chemical exposure. *Basic and Clin. Pharmacol. Toxicol.* 124, 199–210. doi:10.1111/bcpt.13117

Ciofani, G., Genchi, G. G., and Mattoli, V. (2012). ZnO nanowire arrays as substrates for cell proliferation and differentiation. *Mater. Sci. Eng. C* 32, 341–347. doi:10.1016/j.msec.2011.11.001

Cui, H., Liu, Q., Li, R., Wei, X., Sun, Y., Wang, Z., et al. (2020). ZnO nanowire-integrated bio-microchips for specific capture and non-destructive release of circulating tumor cells. *Nanoscale* 12, 1455–1463. doi:10.1039/c9nr07349c

Dai, H. (2001). "Nanotube growth and characterization," in *Carbon nanotubes: synthesis, structure, properties, and applications*. Editors M. S. Dresselhaus, G. Dresselhaus, and P. Avouris (Berlin, Heidelberg: Springer Berlin Heidelberg), 29–53. doi:10.1007/3-540-39947-X_3

Dai, K., Dawson, G., Yang, S., Chen, Z., and Lu, L. (2012). Large scale preparing carbon nanotube/zinc oxide hybrid and its application for highly reusable photocatalyst. *Chem. Eng. J.* 191, 571–578. doi:10.1016/j.cej.2012.03.008

Dineshkumar, B., Krishnakumar, K., Bhatt, A. R., Paul, D., Cherian, J., John, A., et al. (2015). Single-walled and multi-walled carbon nanotubes based drug delivery system: cancer therapy: a review. *Indian J. Cancer* 52, 262–264. doi:10.4103/0019-509x.176720

Gaetani, R., Derevyanchuk, Y., Notargiacomo, A., Pea, M., Renzi, M., Messina, E., et al. (2022). Biocompatibility and connectivity of semiconductor nanostructures for cardiac tissue engineering applications. *Bioengineering* 9, 621. doi:10.3390/bioengineering9110621

Geng, C., Jiang, Y., Yao, Y., Meng, X., Zapien, J. A., Lee, C. S., et al. (2004). Well-Aligned ZnO nanowire arrays fabricated on silicon substrates. *Adv. Funct. Mater.* 14, 589–594. doi:10.1002/adfm.200305074

George, S., Pokhrel, S., Xia, T., Gilbert, B., Ji, Z., Schowalter, M., et al. (2010). Use of a rapid cytotoxicity screening approach to engineer a safer zinc oxide nanoparticle through iron doping. *ACS Nano* 4, 15–29. doi:10.1021/nn901503q

Ghaffari, M., Moztarzadeh, F., and Safavi, M. (2019). A comparative study on the shape-dependent biological activity of nanostructured zinc oxide. *Ceram. Int.* 45, 1179–1188. doi:10.1016/j.ceramint.2018.09.302

Ghannam, H., Chahboun, A., and Turmine, M. (2019). Wettability of zinc oxide nanorod surfaces. *RSC Adv.* 9, 38289–38297. doi:10.1039/C9RA05378F

Hong, H., Shi, J., Yang, Y., Zhang, Y., Engle, J. W., Nickles, R. J., et al. (2011). Cancer-targeted optical imaging with fluorescent zinc oxide nanowires. *Nano Lett.* 11, 3744–3750. doi:10.1021/nl201782m

Imaninezhad, M., Kuljanishvili, I., and Zustiak, S. P. (2017). A two-step method for transferring single-walled carbon nanotubes onto a hydrogel substrate. *Macromol. Biosci.* 17, 1600261. doi:10.1002/mabi.201600261

Imaninezhad, M., Schober, J., Griggs, D., Ruminski, P., Kuljanishvili, I., and Zustiak, S. P. (2018). Cell attachment and spreading on carbon nanotubes is facilitated by integrin binding. *Front. Bioeng. Biotechnol.* 6, 129. doi:10.3389/fbioe.2018.00129

Jorio, A., Saito, R., Hafner, J. H., Lieber, C. M., Hunter, M., McClure, T., et al. (2001). Structural (n,m) determination of isolated single-wall carbon nanotubes by resonant Raman scattering. *Phys. Rev. Lett.* 86, 1118–1121. doi:10.1103/PhysRevLett.86.1118

Kuljanishvili, I., Dikin, D. A., Rozhok, S., Mayle, S., and Chandrasekhar, V. (2009). Controllable patterning and CVD growth of isolated carbon nanotubes with direct parallel writing of catalyst using dip-pen nanolithography. *Small* 5, 2523–2527. doi:10.1002/smll.200900841

Lee, J., Kang, B. S., Hicks, B., Chancellor, T. F., Chu, B. H., Wang, H.-T., et al. (2008). The control of cell adhesion and viability by zinc oxide nanorods. *Biomaterials* 29, 3743–3749. doi:10.1016/j.biomaterials.2008.05.029

Li, M., Lin, D., and Zhu, L. (2013). Effects of water chemistry on the dissolution of ZnO nanoparticles and their toxicity to *Escherichia coli*. *Environ. Pollut.* 173, 97–102. doi:10.1016/J.ENVPOL.2012.10.026

Li, M., Zhu, L., and Lin, D. (2011). Toxicity of ZnO nanoparticles to *Escherichia coli*: mechanism and the influence of medium components. *Environ. Sci. Technol.* 45, 1977–1983. doi:10.1021/es102624t

Li, Z., Persson, H., Adolfsson, K., Oredsson, S., and Prinz, C. N. (2018). Morphology of living cells cultured on nanowire arrays with varying nanowire densities and diameters. *Sci. China Life Sci.* 61, 427–435. doi:10.1007/s11427-017-9264-2

Li, Z., Yang, R., Yu, M., Bai, F., Li, C., and Wang, Z. L. (2008). Cellular level biocompatibility and biosafety of ZnO nanowires. *J. Phys. Chem. C* 112, 20114–20117. doi:10.1021/jp808878p

Liao, C., Jin, Y., Li, Y., and Tjong, S. C. (2020). Interactions of zinc oxide nanostructures with mammalian cells: cytotoxicity and photocatalytic toxicity. *Int. J. Mol. Sci.* 21, 6305. doi:10.3390/ijms21176305

Mardosaitė, R., Jurkeviciute, A., and Rackauskas, S. (2021). Superhydrophobic ZnO nanowires: wettability mechanisms and functional applications. *Cryst. Growth and Des.* 21, 4765–4779. doi:10.1021/acs.cgd.1c00449

Milano, G., D'Ortenzi, L., Bejtka, K., Mandrile, L., Giovannozzi, A. M., Boarino, L., et al. (2018). Tuning ZnO nanowire dissolution by electron beam modification of surface wetting properties. *J. Phys. Chem. C* 122, 8011–8021. doi:10.1021/acs.jpcc.8b01158

Minchenko, O. H., Tsymbal, D. O., Minchenko, D. O., Prylutska, S. V., Cherepanov, V. V., Prylutskyy, Y. I., et al. (2016). Single-walled carbon nanotubes affect the expression of the CCND2 gene in human U87 glioma cells: Einwandige Kohlenstoff-Nanoröhren beeinflussen die Expression des CCND2-Gens in humanen U87 Glioma-Zellen. *Mater. Werkst.* 47, 180–188. doi:10.1002/mawe.201600462

Mohammad Karim, A. (2023). Physics of droplet impact on various substrates and its current advancements in interfacial science: a review. *J. Appl. Phys.* 133, 30701. doi:10.1063/5.0130043

Murali, A., Lokhande, G., Deo, K. A., Brokesh, A., and Gaharwar, A. K. (2021). Emerging 2D nanomaterials for biomedical applications. *Mater. Today* 50, 276–302. doi:10.1016/j.mattod.2021.04.020

Onesto, V., Villani, M., Narducci, R., Malara, N., Imbrogno, A., Allione, M., et al. (2019). Cortical-like mini-columns of neuronal cells on zinc oxide nanowire surfaces. *Sci. Rep.* 9, 4021. doi:10.1038/s41598-019-40548-z

Parikh, S. D., Dave, S., Huang, L., Wang, W., Mukhopadhyay, S. M., and Mayes, D. A. (2020). Multi-walled carbon nanotube carpets as scaffolds for U87MG glioblastoma multiforme cell growth. *Mater. Sci. Eng. C* 108, 110345. doi:10.1016/j.msec.2019.110345

Persson, H., Li, Z., Tegenfeldt, J. O., Oredsson, S., and Prinz, C. N. (2015). From immobilized cells to motile cells on a bed-of-nails: effects of vertical nanowire array density on cell behaviour. *Sci. Rep.* 5 (1), 18535–18612. doi:10.1038/srep18535

Pratt, E. P. S., Damon, L. J., Anson, K. J., and Palmer, A. E. (2021). Tools and techniques for illuminating the cell biology of zinc. *Biochimica Biophysica Acta (BBA) - Mol. Cell Res.* 1868, 118865. doi:10.1016/J.BBAMCR.2020.118865

Qi, S., Yi, C., Ji, S., Fong, C. C., and Yang, M. (2009). Cell adhesion and spreading behavior on vertically aligned silicon nanowire arrays. *ACS Appl. Mater Interfaces* 1, 30–34. doi:10.1021/am800027d

Riemenschneider, M. J., Mueller, W., Betensky, R. A., Mohapatra, G., and Louis, D. N. (2005). *In situ* analysis of integrin and growth factor receptor signaling pathways in human glioblastomas suggests overlapping relationships with focal adhesion kinase activation. *Am. J. Pathology* 167, 1379–1387. doi:10.1016/s0002-9440(10)61225-4

Rudnytska, O. V., Khita, O. O., Minchenko, D. O., Tsymbal, D. O., Yefimova, Y. V., Sliusar, M. Y., et al. (2021). The low doses of SWCNTs affect the expression of proliferation and apoptosis related genes in normal human astrocytes. *Curr. Res. Toxicol.* 2, 64–71. doi:10.1016/j.crtox.2021.02.001

Ryoo, S.-R., Kim, Y.-K., Kim, M.-H., and Min, D.-H. (2010). Behaviors of NIH-3T3 fibroblasts on graphene/carbon nanotubes: proliferation, focal adhesion, and gene transfection studies. *ACS Nano* 4, 6587–6598. doi:10.1021/nn1018279

Schaper, N., Alameri, D., Kim, Y., Thomas, B., McCormack, K., Chan, M., et al. (2021). Controlled fabrication of quality ZnO NWs/CNTs and ZnO NWs/gr heterostructures via direct two-step CVD method. *Nanomater. (Basel)* 11, 1836. doi:10.3390/nano11071836

Sharma, D. K., Shukla, S., Sharma, K. K., and Kumar, V. (2022). A review on ZnO: fundamental properties and applications. *Mater. Today Proc.* 49, 3028–3035. doi:10.1016/j.matpr.2020.10.238

Shooshtari, M., Pahlavan, S., Rahbarpour, S., and Ghafoorifard, H. (2022). Investigating organic vapor sensing properties of composite carbon nanotube-zinc oxide nanowire. *Chemosensors* 10, 205. doi:10.3390/chemosensors10060205

Simon, J., Flahaut, E., and Golzio, M. (2019). Overview of carbon nanotubes for biomedical applications. *Mater. (Basel)* 12, 624. doi:10.3390/ma12040624

Wahab, R., Kaushik, N. K., Verma, A. K., Mishra, A., Hwang, I. H., Yang, Y.-B., et al. (2011). Fabrication and growth mechanism of ZnO nanostructures and their cytotoxic effect on human brain tumor U87, cervical cancer HeLa, and normal HEK cells. *JBIC J. Biol. Inorg. Chem.* 16, 431–442. doi:10.1007/s00775-010-0740-0

Wang, X., Liu, L.-H., Ramström, O., and Yan, M. (2009). Engineering nanomaterial surfaces for biomedical applications. *Exp. Biol. Med.* 234, 1128–1139. doi:10.3181/0904-mr-134

Wong, S., Guo, W.-H., and Wang, Y.-L. (2014). Fibroblasts probe substrate rigidity with filopodia extensions before occupying an area. *Proc. Natl. Acad. Sci.* 111, 17176–17181. doi:10.1073/pnas.1412285111

Yin, L., Zhou, J., Gao, L., Zhao, C., Chen, J., Lu, X., et al. (2017). Characterization and osteogenic activity of SrTiO3/TiO2 nanotube heterostructures on microporous titanium. *Surf. Coatings Technol.* 330, 121–130. doi:10.1016/j.surfcoat.2017.09.075

Zhang, Y., Ram, M. K., Stefanakos, E. K., and Goswami, D. Y. (2012). Synthesis, characterization, and applications of ZnO nanowires. *J. Nanomater.* 2012, 1–22. doi:10.1155/2012/624520

Zhou, W., Bai, X., Wang, E., and Xie, S. (2009). Synthesis, structure, and properties of single-walled carbon nanotubes. *Adv. Mater.* 21, 4565–4583. doi:10.1002/adma.200901071

Zhu, G., Zhou, Y., Wang, S., Yang, R., Ding, Y., Wang, X., et al. (2012). Synthesis of vertically aligned ultra-long ZnO nanowires on heterogeneous substrates with catalyst at the root. *Nanotechnology* 23, 055604. doi:10.1088/0957-4484/23/5/055604